Chapter 13
Relationship Between Three-Dimensional Microstructure and Elastic Properties of Cortical Bone in the Human Mandible and Femur

Paul C. Dechow, Dong Hwa Chung, and Mitra Bolouri

Contents

13.1 Introduction

Observations that bone has grain, or differences in mechanical properties by direction, predate our ability to measure these characteristics. Studies of patterns of trabecular orientation in the femoral head were seminal in forming early hypotheses

P.C. Dechow
Department of Biomedical Sciences, Baylor College of Dentistry, Texas A&M Health Science Center, 3302 Gaston Avenue, Dallas, TX 75254 USA, 214-370-7229
e-mail: pdechow@bcd.tamhsc.edu

C. Vinyard et al. (eds.), *Primate Craniofacial Function and Biology*,
DOI: 10.1007/978-0-387-76585-3_13,

about structure/function relationships in the skeleton (Koch, 1917), and remain of great relevance today. Modern techniques have allowed some studies on craniofacial tissues including investigations into the trabecular structure of the mandibular condyle in pigs (Teng and Herring, 1995, 1996), and in humans (Giesen and van Eijden, 2000). Advances in stereology and, more recently, microCT imaging have provided tools for documenting orientation and structure in trabecular bone.

Material orientation in cortical bone has been more difficult to assess systematically. Gebhardt in 1906 proposed that the three-dimensional functional behavior of mature cortical bone is primarily dependent on the three-dimensional organization of osteons. However, attempts to determine cortical material organization relied on techniques such as split-line patterns on the periosteal surface (for example, Dempster, 1967; or Tappen, 1970), which were influenced by osteon orientation among other factors (Buckland-Wright, 1977). The split-line patterns were thought to reflect directions in which the microstructure of cortical bone was oriented to resist stress. Subsequent research has shown this hypothesis to be incorrect (Buckland-Wright, 1977;Bouvier and Hylander, 1981).

Although there is a large amount of literature on the material properties of cortical bone (for summaries, see Evans, 1973; Currey, 1984; Cowin, 1989; Martin et al., 1998; Guo, 2001), information on material properties in three dimensions is limited. Most studies use mechanical methods to measure the material properties unidirectionally, primarily in the axial direction, or presumed direction of greatest stiffness or strength. Acoustic microscopes and the development of nanoindentation techniques have allowed some characterization of bone material properties at a microstructural and even subosteonal level (Guo, 2001) in multiple directions. However, ultrasonic techniques (Lees, 1982; Katz and Yoon, 1984; Ashman, 1989; Dechow et al., 1993; Kohles et al., 1997; Schwartz-Dabney and Dechow, 2003) using 2–20 MHz transducers remain the best method for the characterization of the anisotropy of apparent elastic moduli of cortical bone at an intermediate or tissue level.

Much controversy exists about which structural features are most important for producing anisotropy in the mechanical characteristics of bone. This problem stems from deficiencies in our knowledge of (1) the basic structure of bone at the molecular, ultrastructural, cellular, and microstructural (tissue) levels and (2) associated developmental processes. At the microstructural level, this problem is important because of the necessity for understanding the link between the bone structure and the mechanical behavior of the skeleton. Yet few tools have been developed for (1) quantifying three-dimensional aspects of bone microstructure and (2) modeling the mechanical impact of variations in this structure. To understand bone anisotropy, questions must be addressed with consideration of the hierarchical structure of bone. At the tissue level, cortical microstructural features that determine anisotropy may include both patterns of (1) porosity and (2) the intrinsic anisotropy of the bone matrix itself.

The link between skeletal function, cortical bone structure, and remodeling must take two factors into consideration. The first is the material properties of bone at

a tissue or microstructural level, as these determine bone deformation in response to load. The second is the tissue-level structure of cortical bone, as this structure is essential for understanding how these patterns reflect chronic loading patterns and how osteocytes arranged in this structure or bone matrix are able to transduce mechanical signals into cellular and tissue response.

Previous investigations suggest that bulk elastic properties of remodeled femoral diaphyseal cortical bone are transversely isotropic with the principal material axis (axis of greatest stiffness) aligned with the anatomical long axis of the bone and the predominant direction of the osteons (Yoon and Katz, 1976; Katz et al., 1984; Lipson and Katz, 1984; Katz and Meunier, 1987). While these conclusions seem reasonable, it is of interest to note that previous investigations have not actually attempted to quantify orientation of the elastic orthotropic axes for femoral cortical bone, although much data are now available for the human mandible (Schwartz-Dabney and Dechow, 2003). Likewise, no work has attempted to quantify the average osteon orientation in cortical bone from any region. Existing references have provided qualitative descriptions of Haversian canal orientations in a few postcranial bones (Cooper et al., 2003; Stout et al., 1999).

The goal of this chapter is to begin an exploration of the relationship between tissue-level structure in cortical bone and the three-dimensional elastic properties of the tissue. To do this, ultrasonic techniques were used to determine the orientation of the principle orthotropic axes in three samples of cortical bone. Techniques of confocal microscopy and microcomputerized tomography (microCT) were used to examine osteonal structure, as reflected by Haversian canal structure, in these same bone samples. The hypothesis is a modification of that of Gebhardt (1906), specifically that the three-dimensional elastic structure of mature cortical bone is primarily dependent on the three-dimensional organization of osteons.

13.2 Materials and Methods

Two disc-shaped specimens (10-mm diameter) were collected from the corpora of a human mandible (Fig. 13.1) on the buccal surface inferior to the first molar. The mandible was from a 62-year-old unembalmed frozen female cadaver. An additional specimen was taken from the flat medial surface of the midshaft of a femur from a 71-year-old embalmed male cadaver. Although embalming has been shown to have a small effect on mechanical properties, such as yield stress, there is even less effect on elastic modulus, especially when measured ultrasonically (Guo, 2001; Currey et al., 1994). In any case, the goal of our study is to compare the orientation of the presumed orthotropic elastic axes to overall osteon orientation in the specimens. While embalming in the femur might have minor effects on elastic properties, it is reasonable to assume that these are unlikely to affect patterns of anisotropy or material orientation (Fig. 13.2) in the bone specimens, although data are not available on this point in the literature.

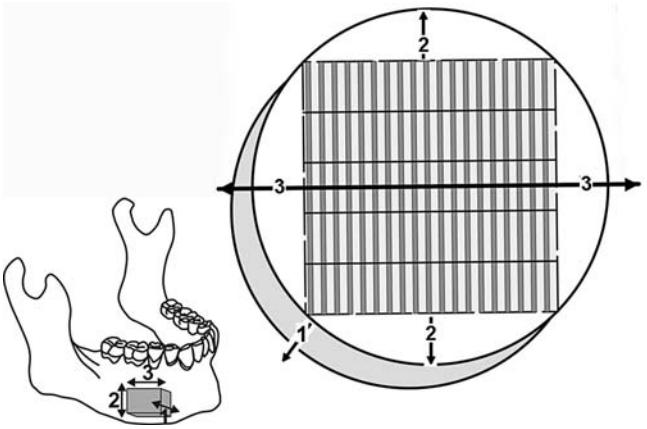

Fig. 13.1 Region of bone sampling for human mandibular bone specimens. The approximate location on the mandibles from which the bone cylinders were removed is illustrated by the box. Following measurement of longitudinal ultrasonic velocities through the diameter and around the perimeter of each cylinder, the axes of minimum and maximum velocity in the cortical plane (which correspond to axes of minimum and maximum stiffness) were used to orient the specimens for reshaping as a block. Both illustrations show the orientation of the axes of the specimens. The "3" direction is that of greatest stiffness in the cortical plane and was approximately parallel to the lower border of the mandible. The "2" direction is that of least stiffness in the cortical plane, and is perpendicular to the "3" direction in cortical plane. The "1" direction is perpendicular to the cortical plane and is in the direction of cortical thickness. The squared structure in the cylinder illustrates the orientation of the serial sections of bone cut with the vibratome. The horizontal lines dividing each vertical white or gray bar in the square into five regions illustrates the relative position of the regions imaged and reconstructed with the confocal microscope. In all, 19 sections (vertical white and gray bars) were cut and five regions or volumes were imaged and reconstructed in each section

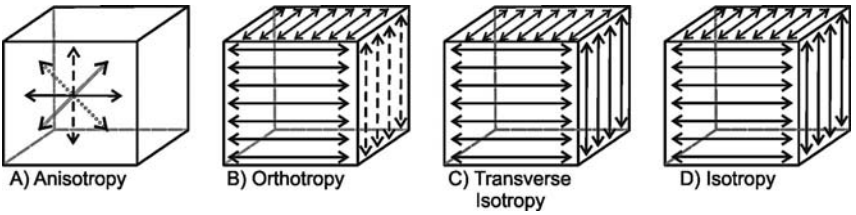

Fig. 13.2 Graphical explanation of material anisotropy. (**A**) In anisotropy, elastic constants differ in all directions with no planes of symmetry. (**B**) In orthotropy, elastic constants vary between three perpendicular planes of symmetry. (**C**) In transverse isotropy, elastic constants are similar in two perpendicular planes, but differ from the third plane. (**D**) In isotropy, elastic properties are the same in all directions

13.2.1 Determination of the Orientation of the Axis of Greatest Stiffness in the Cortical Plane

Longitudinal ultrasonic velocities were measured around the perimeter of each specimen. Prior to harvesting, cortical bone sites were referenced with a graphite line for orientation. The lower border of the mandible and the long axis of the femoral diaphysis were used as reference axes.

Cancellous bone on the inner surface of the specimens was removed with grinding wheels on a water-cooled Tormek grinder or by gentle hand sanding. Bone was cooled continuously with a water drip during preparation. Bone cylinders were harvested from the cortex using a rotary tool (Dremel 732) and 10.0 mm inner-diameter trephine burrs (Ace Dental Implant System). Specimens were stored in a solution of 95% ethanol and isotonic saline in equal proportions. This media has been shown to maintain the elastic properties of cortical bone over time (Ashman et al., 1984; Zioupos and Currey, 1998).

Longitudinal ultrasonic waves were generated by Panametrics transducers (V312-N-SU) resonating at 10 MHz. The transducers were powered with a pulse generator (Hewlett Packard Model 214A). Pulse delays induced by passage of ultrasonic waves through the bone were read on a digitizing oscilloscope (Tektronix TDS420). Velocities were calculated by dividing pulse delays by the specimen width.

First, the bone specimen was attached to the flat top of a dowel (3 mm in diameter) with cyanoacrylate. This dowel was attached to a 4" Rotary Table (P/N 3700, Sherline Products, Inc.), capable of accurate rotations to a tenth of a degree. We then measured the velocities of longitudinal ultrasonic waves passed through the cortical bone for each specimen at 1° angular intervals from 0° to 180°.

A plot of ultrasonic velocities by orientation in an orthotropic material yields a curve resembling a sinusoid if two of the three material axes are in the plane of measurement. The direction corresponding to the apogee is that of greatest stiffness in that plane, and the direction corresponding to the nadir should always be at 90° to the apogee and is the direction of least stiffness. The third material axis would be orthogonal to the first two and thus normal or radial to the plane of the cortical plate (Schwartz-Dabney and Dechow, 2002; Schwartz-Dabney and Dechow, 2003;Ashman et al., 1984; Yoon and Katz, 1976). Tests of ultrasonic velocities through test bone specimens with and without the attachment of the dowel did not show a difference in velocities.

Following collection of the ultrasonic velocities, the data set was fitted to the sinusoidal model using the sinfit function (a least squares fit) in Mathcad Professional (Mathsoft Engineering and Education, Cambridge MA) to generate parameter coefficients for each sine curve. The coefficient of interest here is the angle of the principal axis from the reference line. This describes the direction of the axis of greatest stiffness.

Additional details of the methods for measuring ultrasonic velocities for cortical bone samples have been described previously (Schwartz-Dabney and Dechow, 2003).

13.2.2 Studies of Cortical Structure Using the Confocal Microscope

The three-dimensional microstructure of a cortical bone specimen from the mandible was examined through the use of a confocal microscope (Leica SP2). Attempts to visualize internal structure of undecalcified cortical specimens were unsuccessful because the material was too dense to allow adequate transmission of light, although surface structures can be visualized well without staining.

Before decalcification, a Sherline miniature lathe was used to machine the 10-mm diameter bone cylinder into a squared specimen which was 7 mm × 7 mm × cortical thickness. The square was oriented such that the faces were perpendicular to the material axes, as determined ultrasonically.

After decalcification with EDTA, the unembedded specimen was attached to a block with cyanoacrylate and sectioned at a thickness of 200 μm[1] with a vibrotome (Series 1000 Sectioning System, Technical Products International, Inc., St. Louis, MO). There was little distortion if the specimens remained wet. The sections were immediately attached to a slide with glycerol, placed under a coverslip, and imaged on the confocal microscope. Decalcification did not appear to remove the autofluoresence inherent in the bone tissue, and thus the details were sufficient to reconstruct Haversian canal orientations, and to see some details of osteonal structure.

A series of images at increasing depths using a 10× objective allowed imaging of a volume of 1500 × 1500 × 150 μm^2 (volume of 1024 × 1024 × 102 voxels). These volumes were then reconstructed with a voxel size of 1.47 μm^3, visualized, and measured with Analyze software (AnalyzeDirect, Lenexa, KS). These reconstructions allowed measurement of the orientation of all Haversian canals over the depth of the reconstruction.

The Analyze software package was used to study the splitting patterns, length, and orientations of all Haversian canals within each volume. The canal structures were confirmed as Haversian canals by the visualization of a matrix resembling osteonal structure around each canal. An attempt was made to follow osteons

---

[1] After trials on a number of test bone specimens, in which section thicknesses ranged from 50 μm to 400 μm, a 200 μm thickness for the ultramicrotomed section was found to be optimal for producing a maximum depth for three-dimensional reconstruction. Thicker sections blocked too much light, while thinner specimens restricted the depth of the reconstruction. The vibrotome caused some rippling on the surface of the specimen, which showed up as parallel lines on images taken near the top of the specimen. If the microscope was used to image below the surface, these artifacts were not visible.

[2] A single 1500 × 1500 × 150 μm confocal volume was about 0.28% of the volume of the 7 mm × 7 mm × 2.5 mm cortical bone samples. Each section cut from the sample contained five such adjacent volumes. In total, 19 200 μm thick sections were cut from the bone sample, resulting in 95 reconstructed confocal volumes. These 19 sections and 95 volumes together sampled 35% of the volume of the bone sample, although only 26% could be visualized. There was 9% wastage due to problems associated with reconstructing near the surface of the confocal volumes.

between each of the 19 serial sections. This was successful in many cases, but could not be relied on consistently to reconstruct the entire osteonal tree because of wastage between adjacent sections.

Variation in canal orientation was quantified by determining the angle of each canal within each volume. All angles for all volumes were then combined for study. Thus, if a canal continued on in more than one volume, its angles of orientation would be included as separate observations in the total summary of angles, and by this means weighting for long osteons over the whole specimen was included.

13.2.3 Studies of Cortical Structure Using Micro Computed Tomography

The three-dimensional microstructure of one cortical bone specimen from the mandible and one from the femur were examined through the use of a micro computed tomography (μCT) scanner (μCT 40, ScanCo) at 9 μm nominal isotropic resolution with a 2048 × 2048 pixels image matrix. A miniature lathe (Sherline) was used to machine the 10-mm diameter bone cylinders into rectangular specimens, which were approximately 7 mm × 4 mm × (cortical thickness). The rectangle was oriented such that the 7 mm long axis was in the direction of greatest material stiffness, as determined ultrasonically.

The μCT scanner allowed imaging of the canal structure throughout each cortical bone specimen. Volumetric data from the scanner was imported into Analyze software. Within the software, the specimens were oriented, trimmed, and segmented. Thresholds for segmentation were the same for each specimen and were determined visually so that the maximum amount of canal structure could be seen with a minimum of noise. The software was then used to measure the length and orientation of all canals within each specimen. No attempt was made to measure the diameter of the canals because, to do this, more attention and additional testing would be needed to determine repeatable threshold levels.

Orientations of canals were quantified per unit length of canal. All canals were first divided up manually into approximately straight canal segments. The length and orientation of each of these canal segments were measured within the Analyze environment. For example, for the canal illustrated in Fig. 13.3, the angle and length of the canal relative to the orthogonal axes were determined for the projection of the canal in each of the three planes 12, 13, and 23. Within each plane, the angle was recorded and the length of the canal within the planar projection was used for weighting. In this way, a histogram of the relative orientation of the canals was constructed within each plane. Likewise, canal segments were treated as vectors and trigonometric functions were used to determine the proportion of the vector along each axis (see Fig. 13.3 and lengths of lines 1,2, and 3). These values were then summed for all canal segments to create a comparison of canal orientation along the material axes of the specimens.

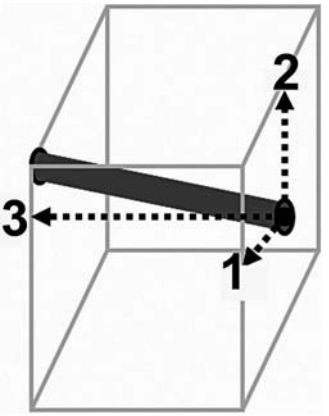

Fig. 13.3 Hypothetical Haversian canal segment within a box oriented to the orthogonal material axes of the cortical bone specimen. The canal segment was treated as a vector and trigonometric functions were used to determine the proportion of the vector along each axis (length of lines 1, 2, and 3). These values were then summed for all canal segments to create a comparison of canal orientation along the material axes of the specimens

13.3 Results

13.3.1 Determination of the Orientation of the Axis of Greatest Stiffness in the Cortical Plane

Plots of ultrasonic velocity by angle in the cortical plane of mandibular and femoral bone specimens reveal a sinusoidal pattern (Fig. 13.4). This pattern is expected in a material that can be approximated as orthotropic.

The primary difference between the femoral and the mandibular specimens in Fig. 13.4 is in the deviation from the idealized curve in the mandibular specimen. At the minimum and especially at the maximum velocities, the curves are flatter and slightly broader than those found in the femoral specimen, indicating a difference in internal microstructure.

13.3.2 Studies of Cortical Structure Using the Confocal Microscope

Confocal microscopy of decalcified mandibular cortical bone thick sections allows unique patterns of visualization of cortical bone microstructure (Figs. 13.5, 13.6). Two hundred and seventy nine osteonal segments were examined in the 95 volumes. These segments varied in length between 0.2 mm (found in two serial sections at most) and 3.8 mm (found in all 19 serial sections) (Fig. 13.6). Actual length could have been longer, because only length in the 3 direction was considered here. Because there were gaps of about 50 μm between serial sections or volumes, it could not be determined if all osteonal canals were connected. However, it is likely that

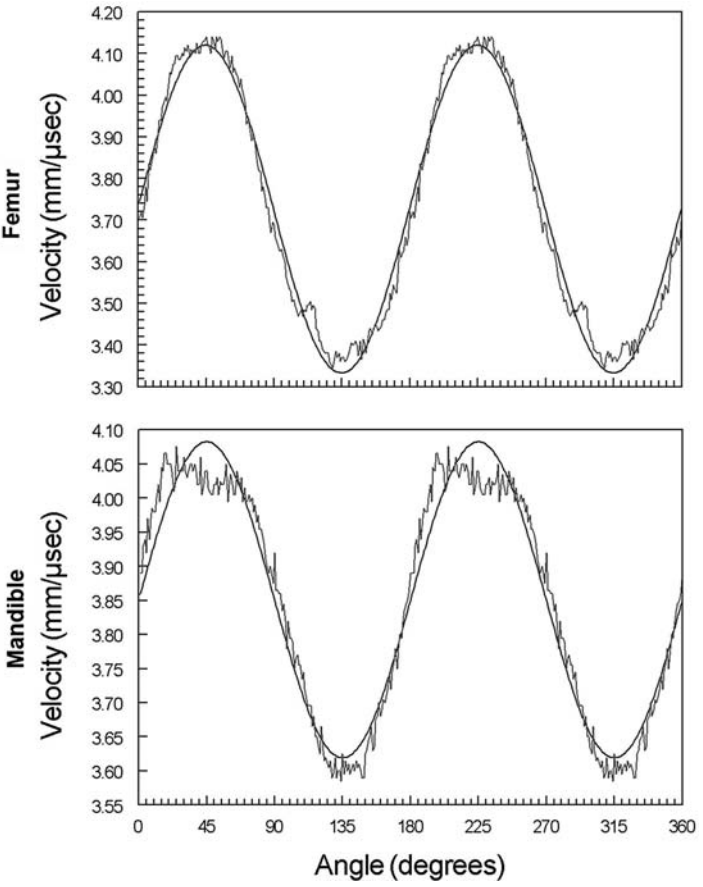

Fig. 13.4 Ultrasonic longitudinal velocities (10 MHz) versus wave direction in the femoral and mandibular specimens used in the µCT portion of the study. Readings were taken at intervals of 1° around the perimeter of the cortical cylinders so that the wave passed through the cortical plane. Peak velocity is the direction of maximum stiffness, and is registered at 45° and 225° for both graphs so that the shapes can be more easily compared. This direction is approximately parallel to the long axis of the femur and the lower border of the mandible respectively. Note the differences in shape in the peaks and the valleys between the femoral and the mandibular specimens

most were, even though these connections were not visualized, because they make up the structure of the vascular bed in the cortical bone tissue. Lamina of cortical bone, or osteonal bone matrix, could be seen around all canal structures, regardless of the orientation of the canal. Likewise, canals without surrounding osteonal matrix were not seen.

Of the 279 osteonal segments, 64 split. These 64 were the longer of the reconstructed canals. The amount of splitting varied from a single splitting in 26 of the 64 to 22 splittings in one osteonal structure. In all, 227 splittings were seen. Of these 207 were bifurcations, 16 were trifurcations and 4 were quadfircations. Thirty one

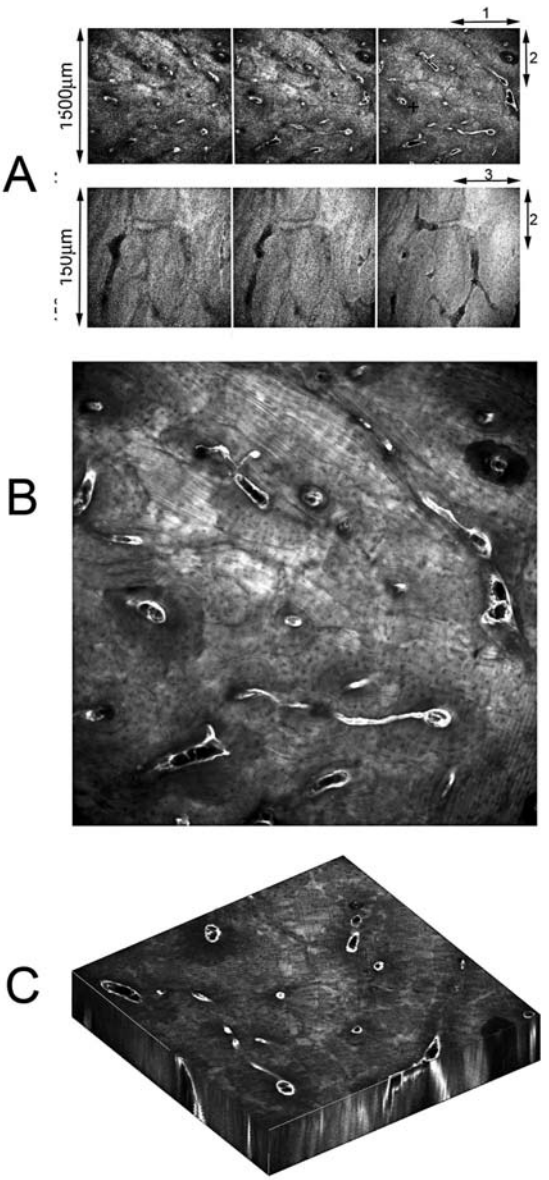

Fig. 13.5 Images of mandibular cortical bone reconstructed from confocal microscope scans. **A**. Reconstructed sections of a single mandibular cortical volume (1 of 95 volumes studied) to show the quality of confocal images taken from a decalcified unstained cortical bone specimen. The top three images are oriented parallel to the 1-2 plane and perpendicular to the 3 (longitudinal) axis. Each section is 1500 ×1500 µm, and the three serial sections are imaged at 15 µm intervals. From this angle, most osteons are seen in cross-section. Close examination of the images reveals changes in canal structure between images. Bone matrix around the canals can also be visualized and varies from faint with indistinct borders (location of cement lines) to very distinct (for example, see the dark osteon in the upper right portion of each photograph or on the left marked with a "+").

osteonal segments rejoined after previous bifurcation. Osteonal matrix surrounding the canals also surrounded the regions of splitting. Daughter branches were most likely to be angled along the long axis of the osteon rather than perpendicular to it. Thus, classic Volksman's canals, which are described in histology textbooks as being perpendicular to longitudinal Haversian canals, were not evident.

Longer osteonal segments were more likely to have multiple splittings than shorter osteonal segments. The correlation coefficient ($r = 0.689$) of the number of nodes with the longitudinal length of the osteonal segment was significant ($P < 0.05$) but moderate, because little splitting was seen in a few of the longer osteonal segments (Fig. 13.7). A diagram of the pattern of splitting in one complex osteonal segment (Fig. 13.8) shows four bifurcations, three trifurcations, and one rejoining.

Rosette histograms of the orientation of all osteonal segments in the three planes of each of the 95 reconstructed confocal volumes all showed a similar pattern. This pattern is illustrated cumulatively for all volumes (Fig. 13.9). The pattern showed that there is a difference between the projection of osteonal orientation in the 2-3 plane compared to the 1-3 plane. This difference can be also be seen in the 1-2 plane projection because more osteonal segments in that plane are oriented along the 2 axis than along the 1 axis. This pattern indicates that osteons vary more in orientation relative to the 3 axis by being oriented up or down (along the 2 axis), rather than in and out through the cortical thickness of the specimen (along the 1 axis).

The mean direction of osteon orientation in the 1-3 plane was 88.8°(Circular SD = 20.6°), which was not significantly different from 90°, or the orientation of maximum stiffness. The mean direction in the 2-3 plane was 95.1° (circular SD = 27.0°), which was significantly different from 90°. This small difference indicated that, on average, the osteons in this plane were oriented 5° above the orientation of maximum stiffness relative to an anterior to posterior vector. Most interesting in this comparison is the larger standard deviation for the angles in the 2-3 plane

Fig. 13.5 (Continued) The bottom three images are also serial sections at 15° μm intervals, but are smaller in size at 150 ×150 μm. These images are parallel to the 2-3 or cortical plane and perpendicular to the direction of cortical thickness. From this orientation, canals appear to be primarily split longitudinally, and faint shadows of osteonal bone matrix can be visualized around the canals. Osteonal splitting can be clearly seen ("*" on lower right figure. **B**. Collapsed confocal image. The region shown is the same as that in the top three images in part A, except here all 100 images of varying depths of the volume are collapsed (added and averaged) to create a single image. This is equivalent to examining an image of a 150 μm thick section, although details from all levels are overlain equally well. In an optical image, there would be a bias toward parts of the volume closer to the lens. In this image, it is much easier to visualize details than in the single sections in **A**. Bone matrix in the osteons is much more distinct. Laminae and osteocyte lacunae can be seen. **C**. Reconstructed volume of mandibular cortical bone. Here canal and osteon structures are also visible and can be seen from three orientations simultaneously. Within Analyze software, this volume can be visually modified to examine and measure internal morphology. The figure gives an indication of how canals and osteons can be followed through the volume and into adjacent volumes.

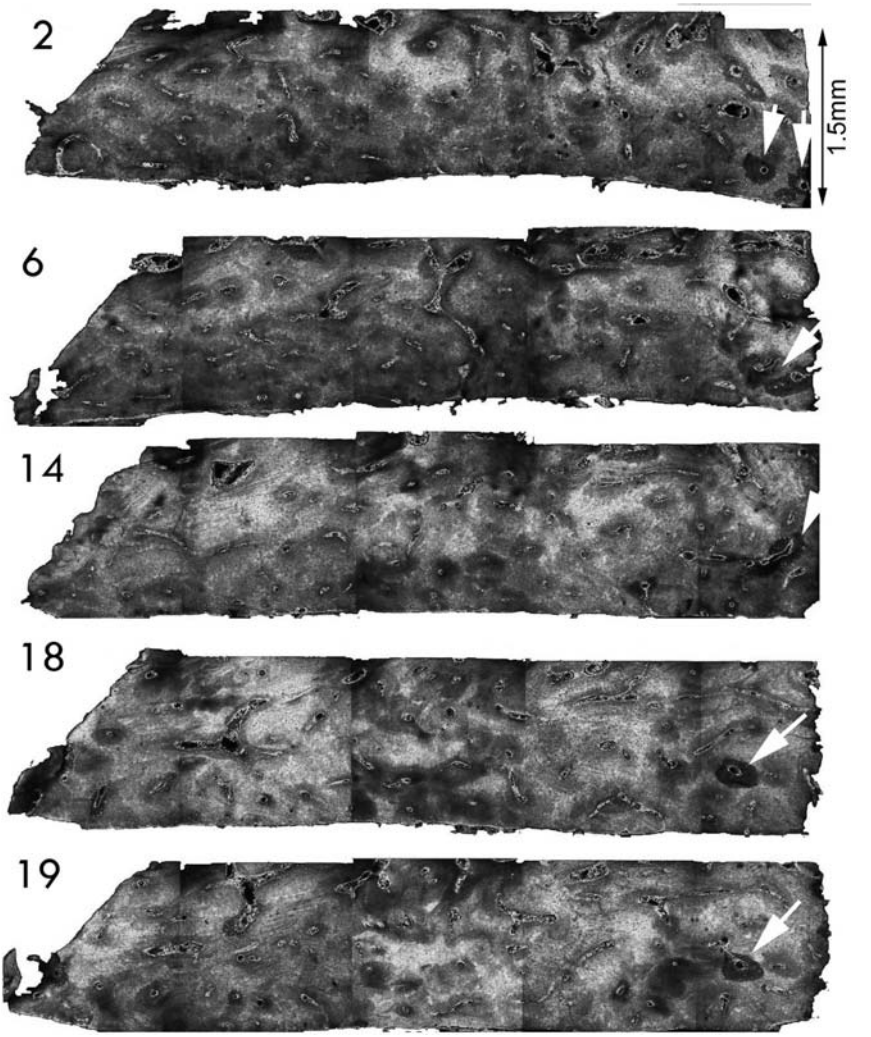

Fig. 13.6 Compilations of collapsed confocal images (all similar to that in Fig. 13.5) to show entire cross-sections of the bone specimen in the 2-3 plane or perpendicular to the 3 or longitudinal axis. Size of each section is about 7.5 × 1.5 mm. Details of canals and osteonal structure are seen in each section and can be followed to adjacent sections. Some osteons run through all 19 sections. For example, the dark osteon on the left (indicated by the white arrows) can be found in all sections. In sections 2 through 14, splitting of the osteon is seen

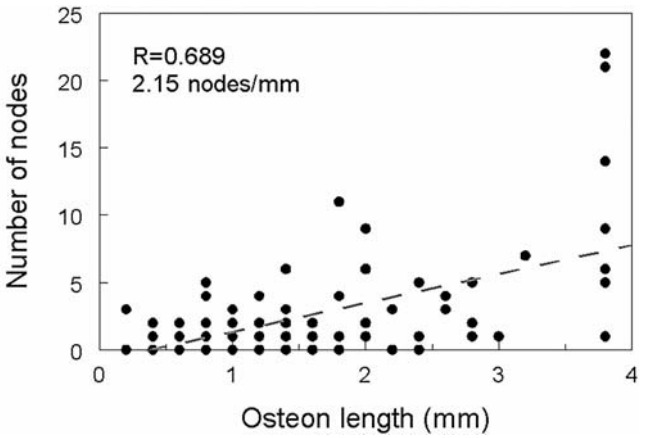

Fig. 13.7 The number of nodes correlates with the longitudinal length of the osteonal segments ($P < 0.05$). This correlation is moderate, and some osteons were found that had few branches despite their relatively long lengths

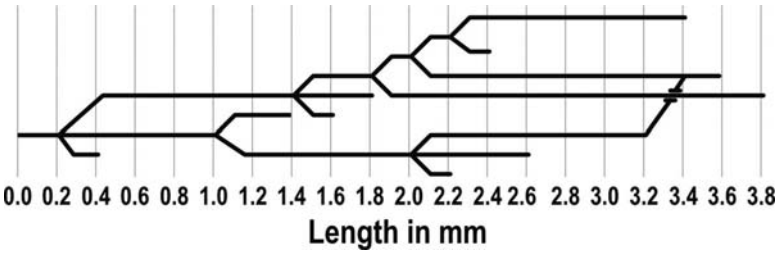

Fig. 13.8 Example of a splitting pattern in a complex osteonal segment. Note that this diagram does not give any details of tertiary structure. Splitting includes bifurcations and trifurcations as well as a rejoining. The Y-axis is not to scale

(Fig. 13.9). This difference is even more evident in other measures of circular statistics, such as concentration[3] (2.6 for 1-3 plane versus 1.7 for the 2-3 plane), and show a greater concentration of angles in the 1-3 plane.

[3] The concentration is a parameter specific to the von Mises distribution, and measures the departure of the distribution from a perfect circle (or a uniform distribution). It is related to the length of the mean vector. The value reported by Oriana Statistical Software is the maximum likelihood estimate of the population concentration, calculated using the formula in Fisher (1993, p. 88) and Mardia and Jupp (2000, pp. 85–6).

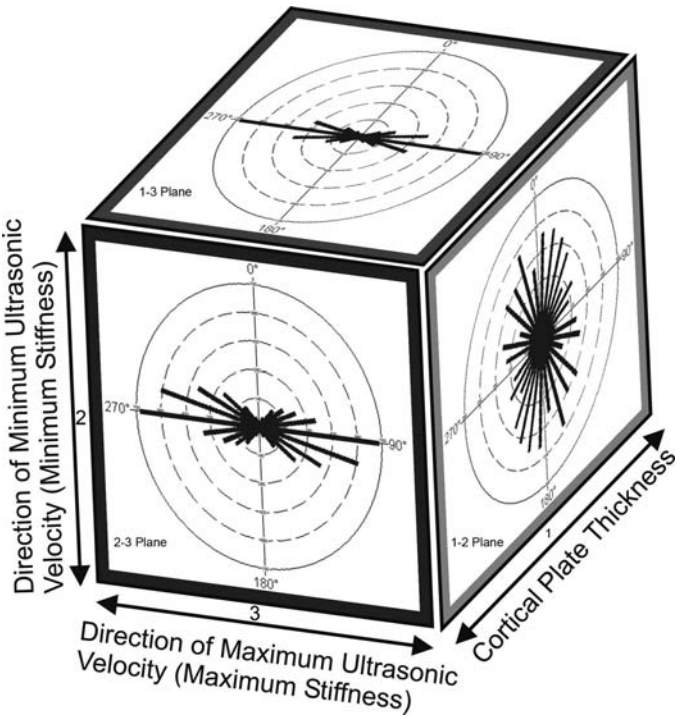

Fig. 13.9 Rosette histograms of angles of all osteonal segments in all 95 reconstructed confocal volumes. The scales for the three histograms are not equivalent and are shown here together in order to focus on the differences in the distributions. If osteonal structure is visualized in the 1-3 plane (histogram at the top of the box), most osteons will appear longitudinally oriented. In the 2-3 plane (histogram on the side of the box), most osteons also appear oriented along the long axis of the mandible, except there is significant variation seen; and many osteons appear oriented at an angle above or below the center line, indicating the direction of maximum stiffness in the cortical plane. When viewed in the 1-2 plane (histogram on the front of the box), osteons appear oriented in all directions, although there are more in the 2 or up-down direction

13.3.3 Studies of Cortical Structure Using Micro Computed Tomography

Reconstructions from μCT imaging showed a much denser canal network for the femoral specimen than for the mandibular specimen (Fig. 13.10). In the femoral specimen, the cumulative length of all canals was 153.0 mm, compared to 67.2 mm in the mandibular specimen. In per cubic millimeter of cortical bone, there were 12.4 mm of Haversian canal length for the femoral specimen versus 5.4 mm for the mandibular specimen.

In both μCT specimens, most osteons appear overall to be oriented in the direction of maximum stiffness, although much deviation is also apparent (Fig. 13.10). Unlike the numerous apparently independent osteonal fragments observed in the

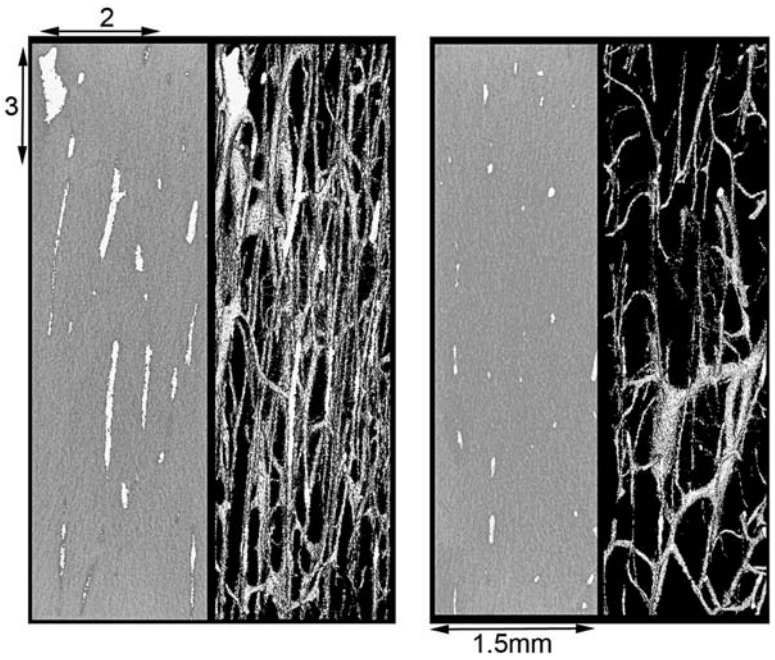

Fig. 13.10 Reconstructions of cortical bone volumes from μCT scans. The two figures on the left are from the femoral specimen and the two figures on the right are from the mandibular specimen. The left figure in each pair is a superficial surface image of the specimens, and the right figure shows the internal canal structures with the matrix removed. The up–down direction for each specimen corresponds with the orientation of maximum stiffness in the plane of the cortical plate (3 direction), and the right–left direction corresponds with the orientation of minimum stiffness in the plane of the cortical plate (2 direction). The size of the imaged regions is 5.5 mm (up–down) by 1.5 mm (*right–left*) by 1.5 mm (deep)

confocal microscope study, all canals examined in the femoral and mandibular μCT specimens were joined. This demonstrated that the networks of osteons in these specimens are each formed by a single vascular bed.

Statistical analysis of osteon orientations weighted by osteon length showed a similar pattern in the mandibular μCT specimen as that found in the confocal microscope mandibular specimen, (Fig. 13.11). In the mandibular μCT specimen, osteons were oriented on average along the axis of greatest stiffness in the 1-3 plane (mean = 94.1°, circular SD = 26.4°). In the 2-3 plane, the average orientation was 30° above an anterior–posterior vector aligned along the orientation of the axis of greatest stiffness (mean = 120.1°, circular SD = 45.9°). The much greater variance in the 2-3 plane compared to the 1-3 plane is evident in Fig. 13.11. This difference is also found in concentration (1-3 plane = 1.8; 2-3 plane = 0.6).

The pattern in the femoral μCT specimen was different. In both the 1-3 and the 2-3 planes, osteons were oriented in the direction of maximum stiffness with less variation in either plane than that found in the mandibular specimens (1-3 plane:

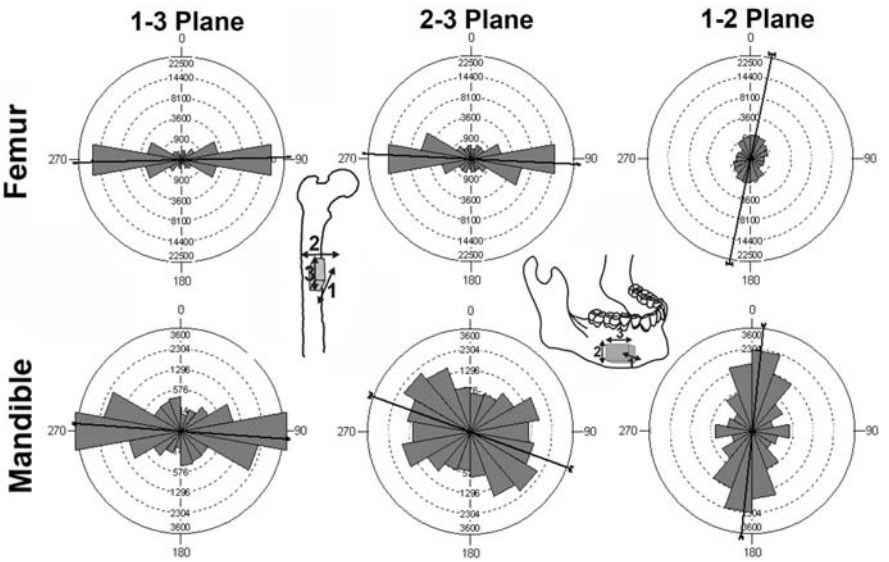

Fig. 13.11 Rosette histograms of the orientations of all osteonal segments per micron length relative to the plane of projection. Angles are weighted by the length of each osteonal segment, and the histograms for each projection within each bone specimen use the same scale. The scale is much larger for the femoral histograms because a much greater number of canals were found in a comparable volume of bone. In the femoral specimen, most osteons are oriented along the axis of greatest stiffness in the cortical plane (3 direction and longitudinal anatomical axis), although there is slightly more variation along the axis of minimum stiffness in the plane of the cortical plate (2 direction) than in the radial direction (1 direction). The mandibular specimen shows a similar pattern, except that the variation in the 1 and 2 directions are much larger relative to the 3 direction. This is especially so for the 2 direction, which corresponds with the tendency of many more osteons to be oriented at angles above or below the 3 axis

mean = 88.4°, circular SD = 13.3°; 2-3 plane: mean = 92.8°, circular SD = 18.4°). Note that there is still a difference in variance between the two planes, but this difference is relatively smaller than that found in the mandibular μCT specimen. The concentrations reflect the greater orientation of the femoral osteons (1-3 plane = 5.2; 2-3 plane = 3.0).

When the canal segments were treated as vectors and trigonometric functions were used to determine the proportion of the vectors along each axis (Fig. 13.3: length of lines 1, 2, and 3), the sum of these values for all canal segments showed a pronounced difference between the mandibular and the femoral μCT specimens. In the mandibular specimen, osteon orientation was 16% in the 1 direction (cortical thickness), 36% in the 2 direction (axis of minimum stiffness in the cortical plane), and 48% in the 3 direction (axis of maximum stiffness in the cortical plane). These values in the femoral specimen were respectively 11%, 16%, and 73%, indicating that osteons are more longitudinally oriented in the femoral specimen than in the mandibular specimen, and that there is a difference between the 1 and 2 axes in the mandibular specimen, which is much less apparent in the femoral specimen.

13.4 Discussion

The goal of this chapter is to explore the relationship between tissue-level structure and three-dimensional elastic properties in cortical bone tissue. The hypothesis is that the three-dimensional elastic structure of remodeled cortical bone at a tissue level of organization is primarily dependent on the three-dimensional organization of osteons (Hert et al., 1994; Skedros et al., 1994). Quantification of the three-dimensional structure of osteons has been an elusive goal due to the difficulty in visualizing internal structure in cortical bone. This study explores two novel technologies, confocal microscopy and μCT, to test how these imaging techniques can be used in quantifying the three-dimensional structure of cortical bone. A key component of this investigation is the use of ultrasound to determine the orientation of the material axes of the cortical bone material. This orientation can be compared to the mean orientation of osteons in a tissue specimen. Differences between regions in cortical bone elastic anisotropy can be compared to differences in the variation of osteonal orientation in these same regions.

13.4.1 Orientation of Elastic Properties in Cortical Bone Tissue

Tissue level elastic properties are necessary for both accurate mechanical models and to understand potential structural adaptations in the craniofacial skeleton (Hart et al., 1992; Korioth and Hannam, 1994a, b; Kabel et al., 1999; Dechow and Hylander, 2000; van Eijden, 2000; Vollmer et al., 2000). For example, local anisotropy and regional variations in skeletal elastic properties can have pronounced effects on the relationship between stress and strain patterns (Carter, 1978; Cowin and Hart, 1990; Cowin et al., 1991; Ricos et al., 1996, Dechow and Hylander, 2000).

Insights into the relationship between mandibular deformation, loading, and the structure of cortical bone can be gained by an examination of strain gage results in light of cortical elastic properties (Dechow and Hylander, 2000). Strain gage studies in the human mandible have demonstrated complex patterns of in vivo (Asundi and Kishen, 2000) and in vitro cortical bone strain (Andersen et al., 1991a, b; Throckmorton et al., 1992; Throckmorton and Dechow, 1994; Yamashita and Dechow, 2000). Studies using animal models suggest similar complexities (Bouvier and Hylander, 1996; Endo, 1973; Hylander, 1979a, b, 1984; Hylander et al., 1987; Marks et al., 1997; Teng and Herring, 1996), which result from variations in skeletal and muscular form and masticatory muscle contraction dynamics (Harper et al., 1997; Hylander and Johnson, 1994; Throckmorton et al., 1990; van Eijden et al., 1990). These variations may have differential effects on various structural and functional regions of the mandible (Dechow and Hylander, 2000; Schwartz-Dabney and Dechow, 2003).

This leads to the hypothesis that functional variations in some regions of the mandible are correlated with an increased variability of elastic properties. Confirmation of this may help elucidate a mechanistic explanation for why certain regions

of the mandible have considerable variation in (1) the orientations of their axes of maximum stiffness and (2) the amount of anisotropy (Schwartz-Dabney and Dechow, 2003). Little is known about those variations in cortical microstructure, which might result in variations in three-dimensional elastic properties of cortical bone. This is especially important at the tissue level because it is the level most relevant to the studies of skeletal biomechanics. Knowledge of structural variation at this level may provide links to understanding functional adaptation within the levels of structural hierarchy of smaller dimension in cortical bone.

At the tissue or supraosteonal level, ultrasonic studies have shown that the elastic structure of mandibular cortical bone was unlike the presumed structure of femoral cortical bone. Mandibular cortical bone in the region of the corpus showed larger differences in ultrasonic velocities and calculated elastic moduli between each of its three orthotropic axes (Schwartz-Dabney and Dechow, 2003). This is a different pattern than has been suggested for the femur and the midshafts of other postcranial long bones.

In the midshafts of long bones, Sevostianov and Kachanov (2000) and Yeni et al. (2001 have shown that theoretical consideration of patterns of porosities (Haversian canals, Volkman's canals, canaliculi, and osteocyte lacunae) can explain much of the basic pattern of cortical bone anisotropy. These theoretical considerations suggest that cortical bone is dominated by longitudinally oriented osteons and can best be modeled as transversely isotropic with the plane of symmetry perpendicular to osteon orientation. Sevostianov and Kachanov (2000) note that studies by Katz et al. (1984) and Ashman et al. (1984) using ultrasonic methods, and Reilly and Burstein (1974) and Zioupos et al. (1995) using mechanical testing, have shown that the cortices of long bones are transversely isotropic as the measures of stiffness normal and tangential to the bone surface usually have values that vary by 10% or less. This is in contrast to elastic moduli in the longitudinal direction, which are 50% or more greater.

This picture differs from cortical anisotropy in the mandible. Our studies (Dechow et al., 1992, 1993; Dechow and Hylander, 2000, Schwartz-Dabney and Dechow, 2003) show orthotropy in the mandible, but not transverse isotropy. However, it is important to note that although the osteonal structure of femoral cortical bone strongly suggests that one axis of orthotropy parallels the long axis of the bone, this assumption has not been tested directly. In the mandible, studies of elastic property orientation in hundreds of cortical specimens (Schwartz-Dabney and Dechow, 2003) have shown variation both between and within regions in material orientation. The specimens in this study come from the lower border of the mandible in the molar region, where such variation is minimal. However, no previous studies have examined such variation in elastic orientation in the shaft of the femur. The specimen studied here showed that, as assumed in the literature, the femur is stiffest directly along its longitudinal axis. Studies on ten other femoral specimens in our laboratory (manuscript in preparation) have shown an identical pattern, and have indicated less variability in the orientation of cortical elastic structure than is found in the mandible.

13.4.2 Orientation of Cortical Bone Tissue Structure

Another problem with applying the theoretical considerations of Sevostianov and Kachanov (2000) is our lack of knowledge of the three-dimensional structure of bone at the tissue level. In particular, information on osteon orientation is both minimal and contradictory. Likewise, despite much research on the material properties of individual osteons, and investigations of variations of collagen structure in osteons, there is little information on the effects of three-dimensional osteon structure on tissue level material properties. Several studies point to contradictions in this area. Studies by Hert et al. (1994) and Petrtyl et al. (1996) review and support earlier work, suggesting that femoral osteons are oriented in opposite off-axis directions in the medial and lateral cortical walls. They suggest that these off-axis orientations, which vary 5°–15° from the long axis of the bone and are not found in atypical (unloaded?) femurs, are aligned with principal stresses resulting from the combination of the predominant compressive, bending, and torsional femoral loads. In contrast, Stout et al. (1999) used biomedical imaging technology (Analyze Software, Mayo Clinic) to create three-dimensional reconstructions of osteons from histological sections of dog femurs, previously described by Tappen (1977). They did not find a spiraling or even off-axis orientation of osteons, as reported in other investigations, but rather a predominately longitudinal organization, but with complex patterns of splitting. It is possible, although uninvestigated, that differences between these studies can be accounted for by several important factors, including probable functional differences between species, differences in visualization techniques, and the size or portion of the bones under study.

The results of this investigation clearly show that, in the femoral specimen, the average orientation of the canals in the cortical bone align very closely with the measured axis of maximum stiffness in the plane of the cortical plate, which in turn has the same orientation as the long axis of the bone. Likewise, variation in osteon orientation in the other two directions is relatively similar, as would be expected in a structure that can be approximated as transversely isotropic. The small difference between these two orientations involved a slightly greater variation in canal orientation in the 2-3 plane compared to the 1-3 plane, indicating more osteonal segments that diverged from the axis of maximum stiffness in the 2 direction than in the 1 direction. This greater variation suggests that, based on osteonal orientation alone, the bone should be slightly stiffer in the 2 direction than in the 1 direction (Ashman et al., 1984).

The difference in stiffness between the 1 and 2 directions in the femur (Ashman et al., 1984) is small compared to that found in the mandible (Schwartz-Dabney and Dechow, 2003). In both of our mandibular specimens, using different types of analysis in each, there was much greater variation in osteonal orientation in the 2-3 plane compared to the 1-3 plane. This difference was the greatest using the results of the mandibular μCT study. In the confocal microscopy study, the sampling was done by quantifying the osteonal segment angles in each of the 95 confocal volumes. Thus a longer osteonal segment in an individual volume that was not aligned in the

direction of maximum stiffness was given the same weight as one aligned in the direction of maximum stiffness. Osteons in this later direction would by definition be shorter because of the orientation of the tissue sections. Thus, the measurement method in the confocal study might have created bias that underestimated the actual difference between the two planes in variability. In any case, the much greater variation in osteon segment orientation in the 2-3 plane compared to the 1-3 plane is what would be expected in a structure that is being modeled as orthotropic.

One problem here though is that the alignment between the axis of maximum stiffness and the mean orientation of the osteons does not correspond as well in the mandibular specimens as in the femoral specimen. In the femoral specimen, the difference is 1.6° in the 1-3 plane and 2.8°in the 2-3 plane, compared respectively to 1.2° and 4.9° in the confocal microscope mandibular specimen, and 4.1° and 30.1° in the μCT mandibular specimen. Even though the large deviance in the 2-3 plane of the μCT mandibular specimen is offset by the large variance in this measurement (Fig. 13.11), it is also clear that the majority of osteons are oriented in an anteroinferior to posterosuperior direction, while the orientation of greatest elastic stiffness is approximately parallel to the mandibular lower border.

It is also interesting in this regard that the ultrasonic curves (Fig. 13.4) for the mandibular specimen showed deviation from the idealized sine curve, especially by flattening at the apex. This pattern has not been found in most mandibular specimens in our laboratory (Schwartz-Dabney and Dechow, 2003), even though most show a pattern of orthotropy (rather than transverse isotropy). However, angular sampling in the 2003 study was insufficient to provide the more nuanced view of the shapes of these curves as described here. The greater density of osteons in the femoral specimen may be important, as the more prevalent non-osteonal interstitial bone may have more of an impact on the elastic structure in this mandibular specimen. Presumably, the interstitial bone is older than the osteonal bone and may reflect a different pattern of deposition and orientation than the osteonal matrix. This could result in increased variation in elastic structure in the mandibular cortical bone specimen.

If anisotropy in tissue elasticity in remodeled cortical bone is primarily dictated by osteonal structure, and osteonal structure has significant splitting, including off-axis, and horizontal components, as shown in this study and also in other investigations, such as those by Stout et al. (1999) in dog femur and in so-called drifting osteons in the midshafts of human metatarsals and baboon fibulas (Robling and Stout, 1999), then it is reasonable to question the limits of the assumption of orthotropy in mandibular cortical bone at a tissue level. For instance, some regions of cortical bone may not have a maximum axis of stiffness, but rather have microstructural components arrayed in a way so that there is equivalent stiffness over a range of angles. This may be the significance of the pattern of variation in the mandibular μCT specimen. But analyses of more specimens are required before any consistent pattern can be suggested. Findings from ultrasonic studies (Schwartz-Debney and Dechow, 2003, and unpublished data) suggest this may be true in some mandibular specimens and is also likely to vary regionally.

13.4.3 Osteonal Morphology in Cortical Bone

It is beyond the scope of this study to comment in detail on the implications for understanding of osteonal morphology. Yet the results do point out some important features. The results show that splitting patterns can be variable with some osteons splitting frequently and having complex networks, while other osteonal segments may travel for longer distances with no apparent splitting.

The results also call into question the significance of so-called Volksman's Canals, or channels that are usually perpendicular to the predominant long axis of osteons. The results show that splitting in osteonal trees occurs over a continuous range of angles from the axis of maximum stiffness to angles perpendicular to this axis. Study of matrix around all canals with confocal microscopy did not reveal channels at any angle that lacked a surrounding distinct matrix or osteonal structure.

Results from the μCT studies called into question the independence of the osteonal segments visualized using confocal microscopy. The canal structures in the μCT specimens were all continuous.

In total, this information suggests that it is important to view osteons in cortical bone as a structured vascular bed, rather than as a series of parallel longitudinal straws, or a series of osteons of variable complexity. The shape of this vascular bed may be affected by biomechanical forces, which likewise affect the three-dimensional aspects of material properties in cortical bone. In this sense, the internal walls of the canal system truly represent a third envelope for resorption, disposition, and potential response to mechanical changes in loading.

It is also logical to ask how the patterns of the vascular beds in cortical bone compare not only between regions but also with such beds in other tissues, which may or may not be subjected to significant loading. There is little data in the literature to even begin making such comparisons.

13.4.4 Elastic Anisotropy, Bone Tissue Structure, and Adaptation

Most studies of the mechanical properties of cortical bone have been concerned with structures at smaller levels of organization, with only a minor emphasis on anisotropy or three-dimensional structure. Variations within osteons and lamellar structures, both within and outside osteons, and a wide array of microarchitectural structures have been suggested to play an important role in mechanical properties (Martin and Burr, 1989; Martin et al., 1998), including the orientation of collagen fibers (Carando et al., 1991; Currey et al., 1994; Riggs et al., 1993) and mineral crystallites (Bacon and Goodship, 1991; Fratzl et al., 1992; Wenk and Heidelbach, 1999). Other investigators have discussed the importance of relative proportions of variable lamellae, containing distinct orientations of collagen fibers and crystallites (Ascenzi, 1988; Fratzl et al., 1993; Turner et al., 1995; Takano et al., 1996; Rinnerthaler et al., 1999). Other matrix factors include mineralization and density (Schaffler and Burr, 1988), as well as the degree of collagen cross-linking (Lees et al., 1990).

Currey and Zioupos (2001) pointed out that anisotropy in cortical bone is dependent on both porous structures and anisotropies within the bone matrix itself. Indeed, most studies that attempt to relate skeletal function with microstructural variation concern themselves with collagen matrix organization, patterns of bone mineralization, and their relationship. However, at a tissue level, which can be related to the mechanics of whole bones, the hierarchical structure of bone must be considered in the assessments of material properties.

At a tissue level, the organization of cortex matrix components, such as the osteons, surface lamellae, and interstitial bone, must be considered in tandem with porous structures. Using X-ray pole figure analysis, Sasaki et al. (1989, 1991) found that anisotropy can be explained by the axial distribution of bone mineral. Hasegawa et al. (1994) came to a similar conclusion by comparing ultrasonic measurements of elastic constants in demineralized bone and in bone with the organic phase removed. Demineralized bone showed no anisotropy; bone without organic phase showed anisotropies proportionate to fresh bone. However, it is unclear how microarchitectural features contribute to the anisotropy of remodeled cortical bone at a tissue or supraosteonal level. Exploration of how such factors play a role requires much more information about their variation in actual bone specimens and the ability to model them within the range of possibilities of osteonal structure.

Katz et al. (1984) demonstrated how remodeling of cortical bone can change elastic properties and their anisotropies. They argued that plexiform bone, constructed of parallel lamellar units, is symmetrical around three mutually perpendicular axes (orthotropy), while haversian bone in transversely symmetrical, that is, elastic constants are identical about two of three axes (transverse isotropy). Remodeling leads to increased symmetry and decreased stiffness. While this is important in the midshafts of long bones, which undergo large amounts of remodeling, its effect in craniofacial bone, with less remodeling, is unclear. Our results here suggest that the lesser amounts of remodeling can lead to differences between the axis of maximum stiffness in bulk tissue specimens and the mean direction of osteon orientation.

Katz et al. (2005) described anisotropy in the mandible as transversely isotropic. On the face of it, this appears to be a contradiction with the findings of Schwartz-Dabney and Dechow, 2003. But it is important to realize that the study of Katz and colleagues measured three-dimensional elastic properties at a smaller level of organization. The study followed longitudinal osteonal structures through the mandible using an acoustic microscope. At the level of a small number of parallel osteonal segments, a finding of transverse isotropy is likely. But in order to get a better idea of tissue organization that is relevant at a whole bone level, it is important to consider the supraosteonal tissue organization itself. When larger bulk specimens are measured ultrasonically, greater differences in ultrasonic velocities between the 1 and 2 directions are apparent, suggesting greater orthotropy. A close examination of the data of Katz and colleagues (2005) does show higher velocities circumferentially than axially, but these differences are not as great as those found with larger specimens.

These findings suggest, but do not directly show, that cortical bone can alter its three-dimensional elastic structure through remodeling. Some investigations have centered on the effects of altered bone strain on bone mass, porosity, mineralization,

and structural integrity of the whole bone (for summary, see Martin et al., 1998). These studies show that, under certain conditions, cortical bone will model over time to increased loads by greater cortical thickness or increased mass, resulting in increased strength. However, interesting questions remain, such as whether bone can adapt by shifts in material properties or by changes in the direction in which it is most resistant to deformation, and to what degree such adaptation might occur.

Lanyon and Rubin (1985) have argued, based on the findings by Woo et al. (1981), that "internal bone remodeling is not an adaptive response to improve the material properties of bone tissue," although it may increase its fatigue life. However, bone modeling on periosteal and endosteal surfaces forms lamellar bone or woven bone (Ascenzi, 1988; Martin and Burr, 1989; Turner et al., 1992), which has variations in microstructural elements, such as collagen fiber or crystallite orientation, that correlate with material properties. Interstitially, drifting osteons or formation and splitting of normal (Type 1) osteons (Robling and Stout, 1999) may also influence bone mechanical properties.

Our work on the material properties in edentulous mandibles (Schwartz-Dabney and Dechow, 2002) suggests that functional changes in the mandible result in changes in material properties. It is reasonable to hypothesize that such changes result from alterations in the pattern of cortical modeling and remodeling. Differences between dentate and edentulous mandibles were site-specific and suggested both increases and decreases in stiffness, altered ratios of anisotropy, and, at a few sites, altered orientations of maximum stiffness, but no changes in apparent density.

Another test of experimental changes in three-dimensional material properties was that of Takano et al. (1999). They used a surgical model in greyhounds in which portions of the ulna were removed to alter loads on the radius. In controls, bone strains were shown to correlate with an indirect measure of collagen orientation (LSI), indicating differences in collagen orientation based on loading pattern. Radii from osteotomized animals showed increases in bone strain in concert with changes in anisotropy ratios in both demineralized and deproteinized tissues. While this experiment showed a change, information was not collected directly on three-dimensional changes in bone matrix structure.

We hypothesize that the microstructural features that account for the differences in three- dimensional elastic properties between the mandible and the mid-diaphysis of bones like the femur include not only the orientation, size (relative area), and density of osteons but also may include other structural features, such as the relative amounts of periosteal lamellar structures. Likewise, regional variations in these features are the likely cause of the heterogeneity in the material properties of the mandible. We suspect that similar heterogeneity would probably be found in the cortices of other bones, both cranial and postcranial, if sufficient studies were attempted. Current work in our laboratory has shown as great or greater variation in material properties within and among bones of the midface and cranium (Peterson and Dechow, 2002, 2003; Peterson et al., 2006).

Acknowledgments Much inspiration for the work contained in this chapter and others from my laboratory have sprung from the publications and work of Bill Hylander. Bill's approaches have pointed to the necessity of many new directions of investigation in evolutionary and functional

morphology. Bone strain as an experimental technique is essential for making sense of primate mastication, but it also calls into focus the material characteristics of skeletal tissue, which in turn raises many issues about development, growth, and adaptation of hard tissues. Bill's work also raises the inherently important issues, often ignored, of the regional and evolutionary significance of variations in function, skeletal structure, mechanics, and adaptation at the tissue level in bone. I thank Bill for his insights and friendship over the years. I am proud to work in a field to which he has added so much.

Thanks to Dr. Qian Wang for reading and commenting on an earlier version of this manuscript. Thanks also to Drs. Mathew Ravosa, Chris Vinyard, and Chris Wall for their comments on this manuscript and for organizing this outstanding symposium and book dedicated to the growing field of research that stems from the seminal studies of Dr. William Hylander.

References

Andersen KL, Mortensen HT, Pedersen EH, Melsen B. (1991a) Determination of stress levels and profiles in the periodontal ligament by means of an improved three-dimensional finite element model for various types of orthodontic and natural force systems. J Biomed Eng 13:293–303.

Andersen KL, Pedersen EH, Melsen B. (1991b) Material parameters and stress profiles within the periodontal ligament. Am J Orthod Dentofacial Orthop 99:427–40.

Ascenzi A. (1988) The micromechanics versus the macromechanics of cortical bone–a comprehensive presentation. Journal of Biomechanical Engineering 110:357–63.

Ashman RB. (1989) Experimental techniques. In: Cowin SC, (editors), Bone Mechanics, Boca Raton, Florida: CRC Press, Inc. pp. 75–96.

Ashman RB, Cowin SC, Van Buskirk WC, et al. (1984) A continuous wave technique for the measurement of the elastic properties of cortical bone. J Biomech 17:349–61.

Asundi A, Kishen, A. (2000) A strain gauge and photoelastic analysis of in vivo strain and in vitro stress distribution in human dental supporting structures. Arch Oral Biol 45:543–50.

Bacon GE, Goodship AE. (1991) The orientation of the mineral crystals in the radius and tibia of the sheep, and its variation with age. J Anat 179:15–22.

Bouvier M, Hylander WL. (1981) The relationship between split-line orientation and in vivo bone strain in galago (*G.crassicaudatus*) and macaque (*Macaca mulatta* and *M. fascicularis*) mandibles. Am J Phys Anthropol 56:147–56.

Bouvier M, Hylander WL. (1996) The mechanical or metabolic function of secondary osteonal bone in the monkey *Macaca fascicularis*. Arch Oral Biol 41:941–50.

Buckland-Wright JC. (1977) The nature of split-line formation in bone. Proceedings of the Anatomical Society of Great Britain and Ireland.

Carando S, Portigliatti-Barbos M, Ascenzi A, et al. (1991) Macroscopic shape of, and lamellar distribution within, the upper limb shafts, allowing inferences about mechanical properties. Bone 12:265–9.

Carter DR. (1978) Anisotropic analysis of strain rosette information from cortical bone. J Biomech 11:199–202.

Cooper DMI, Turinsky AL, Sensen CW, Hallgrimsson B. (2003) Quantitative 3D analysis of the canal network in cortical bone by micro-computed tomography. Anat Rec 274B: 169–179.

Cowin SC. (1989) The mechanical properties of cortical bone tissue. In: Cowin SC, (editor), Bone Mechanics, CRC Press, Inc. Boca Raton, Florida, pp. 97–128.

Cowin SC, Hart RT. (1990) Errors in the orientation of the principal stress axes if bone tissue is modeled as isotropic. J Biomech 23:349–52.

Cowin SC, Sadegh AM, Luo GM. (1991) Correction formulae for the misalignment of axes in the measurement of the orthotropic elastic constants. J Biomech 24:637–41.

Currey JD. (1984) The mechanical adaptations of bones. Princeton University Press, Princeton, NJ.

Currey JD, Brear K, Zioupos P. (1994) Dependence of mechanical properties on fibre angle in narwhal tusk, a highly oriented biological composite. J Biomech 27:885.
Currey JD, Zioupos P. (2001) The effect of porous microstructure on the anisotropy of bone-like tissue: a counterexample. J Biomech 34:707–10.
Dechow PC, Nail GA, Schwartz-Dabney CL, Ashman RB. (1993) Elastic properties of human supraorbital and mandibular bone. Am J Phys Anthropol 90:291–306.
Dechow PC, Schwartz-Dabney CL, Ashman RB. (1992) Elastic properties of the human mandibular corpus. In: Carlson DS, Goldstein SA, (editors), Bone Biodynamics in Orthodontic and Orthopedic Treatment, Craniofacial Growth Series, Volume 27, Center for Human Growth and Development, The University of Michigan: Ann Arbor, Michigan, pp. 299–314.
Dechow PC, Hylander WL. (2000) Elastic properties and masticatory bone stress in the macaque mandible. Am J Phys Anthropol 112:553–74.
Dempster WT. (1967) Correlation of types of cortical grain structure with architectural features of the human skull. Amer J Anat 120:7–32.
Endo B. (1973) Stress analysis on the facial skeleton of gorilla by means of the wire strain gauge method. Primates 14:37–45.
Evans FG. (1973) Mechanical Properties of Bone. Charles C. Thomas, Springfield, IL.
Fisher NI. (1993) Statistical Analysis of Circular Data. Cambridge University Press, Cambridge. 277pp.
Fratzl P, Fratzl-Zelman N, Klaushofer K. (1993) Collagen packing and mineralization. An x-ray scattering investigation of turkey leg tendon. Biophys J 64:260–6.
Fratzl P, Groschner M, Vogl G, et al. (1992) Mineral crystals in calcified tissues: a comparative study by SAXS. J Bone Min Res 7:329–34.
Gebhardt W. (1906) Über funktionell wichtige Anordnungsweisen der feineren und gröberen Bauelemente des Wirbeltierknochens. II. Spezieller Teil.: Der Bau der Haversschen Lamellensysteme und seine funktionelle Bedeutung. Arch Entw Mech Org 20:187–322.
Giesen EB, van Eijden TM. (2000) The three-dimensional cancellous bone architecture of the human mandibular condyle. J Dent Res 79:957–63.
Guo E. (2001) Mechanical properties of cortical bone and cancellous bone tissue. In Cowin SC (editor) Bone Mechanics Handbook, Second Edition, CRC Press, Boca Raton, pages 10–1 to 10–23.
Harper RP, de Bruin H, Burcea I. (1997) Muscle activity during mandibular movements in normal and mandibular retrognathic subjects. J Oral Maxillofac Surg 55:225–33.
Hart RT, Hennebel VV, Thongpreda N, et al. (1992) Modeling the biomechanics of the mandible – a three- dimensional finite element study. J Biomechanics 25:261–86.
Hasegawa K, Turner CH, Burr DB. (1994) Contribution of collagen and mineral to the elastic anisotropy of bone. Calcif Tissue Int 55:381–6.
Hert J, Fiala P, Petrtyl M. (1994) Osteon orientation of the diaphysis of the long bones in man. Bone 15:269–77.
Hylander WL. (1979a) An experimental analysis of temporomandibular joint reaction force in Macaques. Am J Phys Anthropol 51:433–56.
Hylander WL. (1979b) Mandibular function in Galago crassicaudatus and Macaca fascicularis: an in vivo approach to stress analysis of the mandible. J Morphol 159:253–96.
Hylander WL. (1984) Stress and strain in the mandibular symphysis of primates: a test of competing hypotheses. Am J Phys Anthropol 64:1–46.
Hylander WL, Johnson KR. (1994) Jaw muscle function and wishboning of the mandible during mastication in macaques and baboons. Am J Phys Anthropol 94:523–47.
Hylander WL, Johnson KR, Crompton AW. (1987) Loading patterns and jaw movements during mastication in Macaca fascicularis: a bone-strain, electromyographic, and cineradiographic analysis. Am J Phys Anthropol 72:287–314.
Kabel J, van Rietbergen B, Odgaard A, Huiskes R. (1999) Constitutive relationships of fabric, density, and elastic properties in cancellous bone architecture. Bone 25:481–6.
Katz JL, Meunier A. (1987) The elastic anisotropy of bone. J Biomech 20:1063–70.

Katz JL, Yoon HS. (1984) The structure and anisotropic mechanical properties of bone. IEEE Trans Biomed Eng 31:878–84.
Katz JL, Kinney JH, Spencer P, Wang Y, Fricke B, Walker MP, Friis EA. (2005) Elastic anisotropy of bone and dentitional tissues. J Mater Sci Mater Med. 16:803–6.
Katz JL, Yoon HS, Lipson S, Maharidge R, Meunier A, Christel P. (1984) The effects of remodeling on the elastic properties of bone. Calcif Tissue Int 36:Suppl 1:S31–6.
Koch JC. (1917) The laws of bone architecture. Am J Anat 21:177–297.
Kohles SS, Bowers JR, Vailas AC, Vanderby R Jr. (1997) Ultrasonic wave velocity measurement in small polymeric and cortical bone specimens. J Biomech Eng 119:232–6.
Korioth TWP, Hannam AG. (1994a) Deformation of the human mandible during simulated tooth clenching. J Dent Res 73:56–66.
Korioth TWP, Hannam AG. (1994b) Mandibular forces during simulated tooth clenching. J Orofac Pain 8:178–89.
Lanyon LE, Rubin CT. (1985) Functional adaptation in skeletal structures. In: Hildebrand M, Bramble DM, Liem KF, Wake DB, (editors), Functional Vertebrate Morphology, The Belknap Press of Harvard University Press: London, England, pp. 1–25.
Lees S. (1982) Ultrasonic measurements of deer antler, bovine tibia and tympanic bulla. J Biomech 15:867–74.
Lees S, Eyre DR, Barnard SM. (1990) BAPN dose dependence of mature crosslinking in bone matrix collagen of rabbit compact bone: corresponding variation of sonic velocity and equatorial diffraction spacing. Connect Tissue Res 24:95–105.
Lipson SF, Katz JL. (1984) The relationship between elastic properties and microstructure of bovine cortical bone. J Biomech 17:231–40.
Mardia KV, Jupp PE. (2000) Statistics of Directional Data. 2nd Edition. John Wiley & Sons, Chicester. 429pp.
Marks L, Teng S, Artun J, Herring S. (1997) Reaction strains on the condylar neck during mastication and maximum muscle stimulation in different condylar positions: an experimental study in the miniature pig. J Dent Res 76:1412–20.
Martin RB, Burr DB. (1989) Structure, function, and adaptation of compact bone. Raven Press, New York.
Martin RB, Burr DB, Sharkey NA. (1998) Skeletal Tissue Mechanics. Springer, New York.
Peterson J, Dechow PC. (2002) Material properties of the inner and outer cortical tables of the human parietal bone. Anat Rec 268:7–15.
Peterson J, Dechow PC. (2003) Material properties of the cranial vault and zygoma. Anat Rec 274A:785–797.
Peterson J, Wang Q, Dechow PC. (2006) Material properties of the dentate maxilla. Anat Rec, 288A:962–972.
Petrtyl M, Hert J, Fiala P. (1996) Spatial organization of the haversian bone in man. J Biomech 29:161–9.
Reilly DT, Burstein AH. (1974) The mechanical properties of cortical bone. J Bone Joint Surg (AM) 56-A:1001–22.
Ricos V, Pedersen DR, Brown TD, Ashman RB, Rubin CT, Brand RA. (1996) Effects of anisotropy and material axis registration on computed stress and strain distributions in the turkey ulna. J Biomech 29:261–7.
Riggs CM, Vaughan LC, Evans GP, et al. (1993) Mechanical implications of collagen fibre orientation in cortical bone of the equine radius. Anat Embryol 187:239–48.
Rinnerthaler S, Roschger P, Jakob HF, Nader A, Klaushofer K, Fratzl P. (1999) Scanning small angle X-ray scattering analysis of human bone sections. Calcif Tissue Int 64: 422–9.
Robling AG, Stout SD. (1999) Morphology of the drifting osteon. Cells Tiss Org 164:192–204.
Sevostianov I, Kachanov M. (2000) Impact of the porous microstructure on the overall elastic properties of the osteonal cortical bone. J Biomech 33:881–8.
Sasaki N, Ikawa T, Fukuda A. (1991) Orientation of mineral in bovine bone and the anisotropic mechanical properties of plexiform bone. J Biomech 24:57–62.

Sasaki N, Matsushima N, Ikawa T, et al. (1989) Orientation of bone mineral and its role in the anisotropic mechanical properties of bone- transverse anisotropy. J Biomech 22:157–64.
Schaffler MB, Burr DB. (1988) Stiffness of compact bone: effects of porosity and density. J Biomech 21:13–6.
Schwartz-Dabney CL, Dechow PC. (2002) Edentulation alters material properties of mandibular cortical bone. J Dent Res 81:613–617.
Schwartz-Dabney CL, Dechow PC. (2003) Variations in cortical material properties throughout the human dentate mandible. Am J Phys Anthropol 120:252–77.
Skedros JG, Mason MW, Bloebaum RD. (1994) Differences in osteonal micromorphology between tensile and compressive cortices of a bending skeletal system: indications of potential strain-specific differences in bone microstructure. Anat Rec 239:405–13.
Stout SD, Brunsden BS, Hildebolt CF, Commean PK, Smith KE, Tappen NC. (1999) Computer-assisted 3D reconstruction of serial sections of cortical bone to determine the 3D structure of osteons. Calcif Tissue Int 65:280–4.
Takano Y, Turner CH, Burr DB. (1996) Mineral anisotropy in mineralized tissues is similar among species and mineral growth occurs independently of collagen orientation in rats: results from acoustic velocity measurements. J Bone Miner Res 11:1292–301.
Takano Y, Turner CH, Owan I, Martin RB, Lau ST, Forwood MR, Burr DB. (1999) Elastic anisotropy and collagen orientation of osteonal bone are dependent on the mechanical strain distribution. J Orthop Res 17:59–66.
Tappen NC. (1970) Main patterns and individual differences in baboon skull split-lines and theories of causes of split-line orientation in bone. Am J Phys Anthropol 33:61–72.
Tappen NC. (1977) Three-dimensional studies on resorption spaces and developing osteons. Am J Anat. 149:301–17.
Teng S, Herring SW (1995) A stereological study of trabecular architecture in the mandibular condyle of the pig. Arch Oral Biol 40:299–310.
Teng S, Herring SW. (1996) Anatomic and directional variation in the mechanical properties of the mandibular condyle in pigs. J Dent Res 75:1842–50.
Throckmorton GS, Dechow PC. (1994) In vitro strain measurements in the condylar process of the human mandible. Archs Oral Biol 39:853–67.
Throckmorton GS, Ellis E, III, Winkler AJ, Dechow PC. (1992) Bone strain following application of a rigid bone plate: an in-vitro study in human mandibles. J Oral Maxillofac Surg 50:1066–73.
Throckmorton GS, Groshan GJ, Boyd SB. (1990) Muscle activity patterns and control of temporomandibular joint loads. J Prosthet Dent 63:685–95.
Turner CH, Chandran A, Pidaparti RM. (1995) The anisotropy of osteonal bone and its ultrastructural implications. Bone 17:85–9.
Turner CH, Woltman TA, Belongia DA. (1992) Structural changes in rat bone subjected to long-term, in vivo mechanical loading. Bone 13:417–22.
van Eijden TM. (2000) Biomechanics of the mandible. Crit Rev Oral Biol Med 11:123–36.
van Eijden TM, Brugman P, Weijs WA, Oosting J. (1990) Coactivation of jaw muscles: recruitment order and level as a function of bite force direction and magnitude. J Biomech 23:475–85.
Vollmer D, Meyer U, Joos U, Vegh A, Piffko J. (2000) Experimental and finite element study of a human mandible. J Craniomaxillofac Surg 28:91–6.
Wenk HR, Heidelbach F. (1999) Crystal alignment of carbonated apatite in bone and calcified tendon: results from quantitative texture analysis. Bone 24:361–9.
Woo SL-Y, Kuel SC, Amiel DG, Hayes WC, White FC, Akeson WH. (1981) The effect of prolonged physical training on the properties of lone bone: a study of Wolff's law. J Bone Joint Surg (AM) 63-A:780–7.
Yamashita J, Dechow PC. (2000) Strain patterns of the human mandible during artificial loading. J Dent Res 79, Special Issue: Abstract 2833.
Yeni YN, Vashishth D, Fyhrie DP. (2001) Estimation of bone matrix apparent stiffness variation caused by osteocyte lacunar size and density. J Biomech Eng 123:10–7.

Yoon HS, Katz JL (1976) Ultrasonic wave propagation in human cortical bone-I. Theoretical considerations for hexagonal symmetry. J Biomech 9:407–12.

Zioupos P, Currey D. 1998. Changes in the stiffness, strength, and toughness of human cortical bone with age. Bone 22:57–66.

Zioupos P, Currey JD, Mirza MS, Barton DC. (1995) Experimentally determined microcracking around a circular hole in a flat plate of bone: comparison with predicted stresses. Philos Trans R Soc Lond B Biol Sci 347:383–96.